scientific data

OPEN

DATA DESCRIPTOR

A large open access dataset of transillumination imaging toward the realization of optical computed tomography

To Ni Phan Van[1,6], Hoang Nhut Huynh[2,3,6], Ngoc An Dang Nguyen[2,3], Trung Nghia Tran[2,3]✉ & Koichi Shimizu[1,4,5]✉

Transillumination imaging is commonly used in medicine and biometrics to provide non-invasive insights into internal structures. However, the prevalent image blurring resulting from scattering effects poses a significant challenge to the effective application of transillumination. Artificial intelligence algorithms have gained prominence for enhancing transillumination images and addressing challenges such as scattering suppression, depth estimation, and three-dimensional structure reconstruction. These advances require high-quality input images to optimize model performance. Acquiring a large-scale transillumination image dataset for practical AI applications is difficult due to subjective imaging conditions. This study aimed to overcome this obstacle by introducing a comprehensive dataset of transillumination images. Methods and algorithms for generating depth-dependent point-spread function and transillumination images were presented. The dataset comprised 12,000 pairs of images of clear and scattered media, each associated with the corresponding depth information. This study is valuable for advancing AI-based solutions in transillumination imaging and provides a foundation for further research on image deblurring, depth perception, and 3D reconstruction.

Background & Summary

Fluorescence imaging is known to be effective in imaging internal structures, but this method depends on the light source and the injected excitation agent[1–3]. Therefore, the method using transmitted light is considered an effective alternative. Transillumination imaging is becoming increasingly useful in medical and biometric applications[2,4–7]. This safe technique allows non-invasive body measurements using simple, compact equipment[8]. However, this method has not been widely used in practice. Transillumination images are blurred due to the scattering effects in biological tissue media[9].

Previous studies have attempted to eliminate this effect, such as the depth-dependent Point Spread Function (PSF) proposed by Shimizu *et al*., which simulates the fluorescence structure in a scattering medium[10]. Tran *et al*. proposed a deblurring technique and estimated the depth of the absorption structure by deconvolution using a PSF[11]. Recently, artificial intelligence has emerged as a useful tool for image processing applications[12]. Taking advantage of these advances, Van *et al*. proposed a scatter deblurring and depth estimation technique using deep learning models of Fully Convolutional Network (FCN) and Convolutional Neural Network (CNN) with pairs of original and blurred image data and depths ranging from 0.1 mm to 10.0 mm[13]. Dang and Hoang, *et al*. proposed a technique of pixel-to-pixel scanning and scatter deblurring using a CNN model with multidimensional data and depths from 0.1 mm to 100.0 mm and used the information to reconstruct the structure 3D from 2D images[14–16]. Figure 1 shows an overview of the progress and applications of transillumination imaging.

[1]Graduate School of Information, Production and Systems, Waseda University, Kitakyushu, 808-0135, Japan. [2]Laboratory of Laser Technology, Faculty of Applied Science, Ho Chi Minh City University of Technology (HCMUT), 268 Ly Thuong Kiet Street, District 10, Ho Chi Minh City, 72409, Vietnam. [3]Vietnam National University Ho Chi Minh City, Linh Trung Ward, Thu Duc, Ho Chi Minh City, 71308, Vietnam. [4]Information, Production and Systems Research Center, Waseda University, Kitakyushu, 808-0135, Japan. [5]School of Optoelectronic Engineering, Xidian University, Xi'an, 710071, China. [6]These authors contributed equally: To Ni Phan Van, Hoang Nhut Huynh. ✉e-mail: ttnghia@hcmut.edu.vn; shimizu73@gmail.com

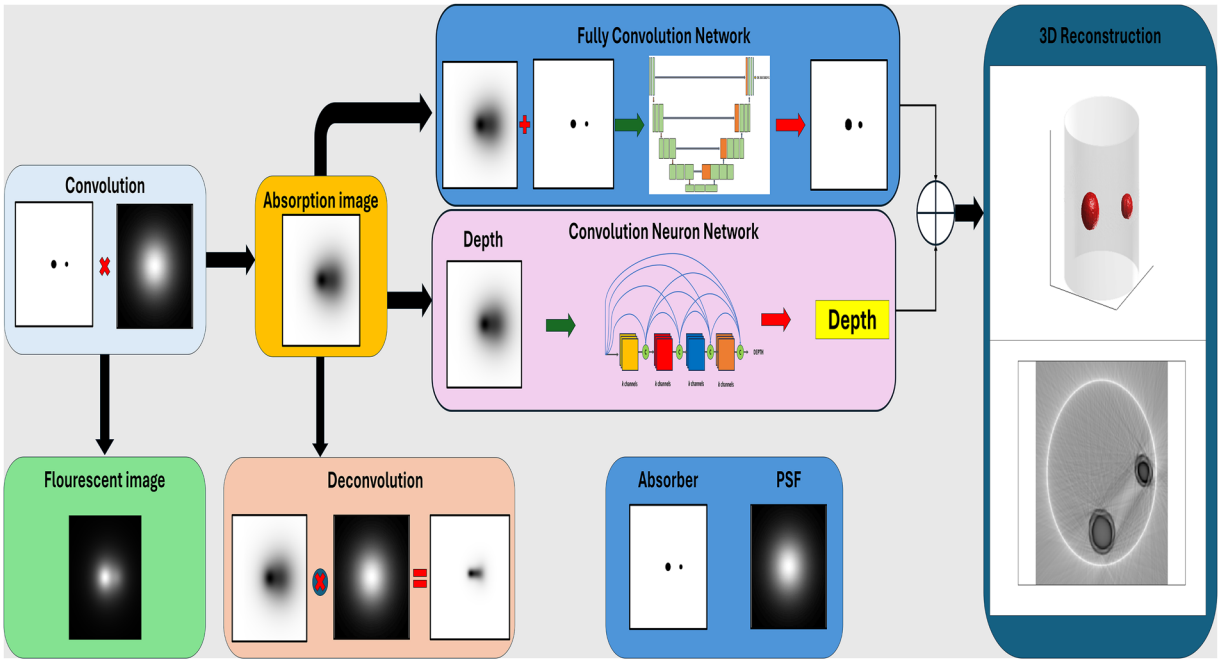

Fig. 1 Overview of progress and applications of transillumination imaging.

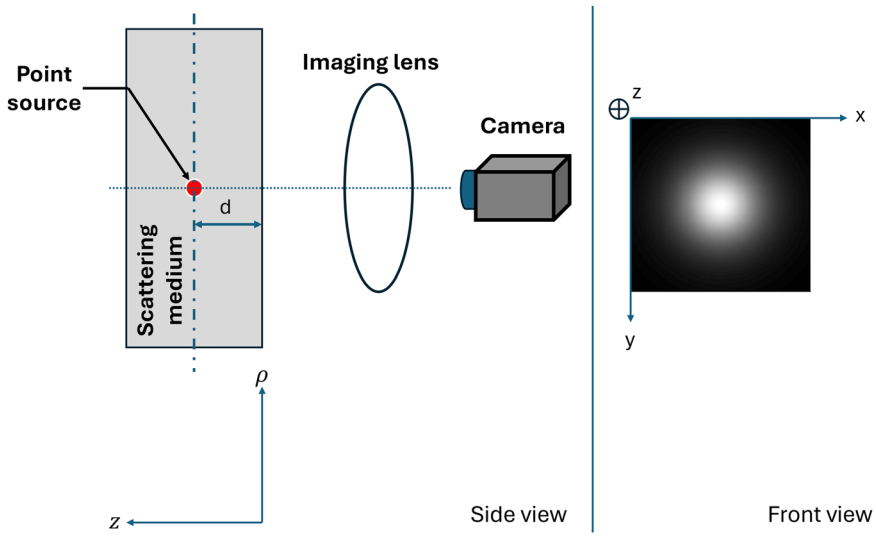

Fig. 2 Geometry of a PSF representing light distribution at scattering medium surface.

The problem with the deep learning method is related to large observed data. Real observed data collection is affected by many factors, such as environmental and image acquisition conditions, leading to data with low reliability and repeatability[13,17]. Therefore, building the dataset from the numerical method by convolving the object structure in a transparent medium with the depth-dependent PSF to simulate the absorption structure in a scattering medium under specified conditions is an initial step.

This study presents a method for generating a dataset from transillumination imaging, such as depth-dependent PSF, simulation of absorption structures in scattering media, and a dataset with multiple depths, sizes, and absorbances to ensure diversity in the data dimensions. In addition, this study presents a method for suppressing background inhomogeneity to ensure that the light illuminates evenly over a sufficient area around the absorbing object. A sample dataset of 12,000 pairs of images is provided in air and scattering environments with corresponding depths.

Methods

Depth-dependent Point Spread Function. In a previous study, a depth-dependent PSF was developed to characterize the blurring effect caused by the scattering of a fluorescent point source in a slab scattering medium. The PSF was calculated under the assumption that the surface of the scattering medium is flat. The spatial distribution of light intensity for a point source is described by Equation (1)[10] and Fig. 2 shows the geometry of the PSF representing light distribution at the surface of the scattering medium.

$$\mathrm{PSF}\,(\rho) = \frac{3P_0}{(4\pi)^2}\left(\mu_s' + \mu_a + \left[\kappa_d + \frac{1}{(\rho^2 + d^2)^{1/2}}\right]\frac{d}{(\rho^2 + d^2)^{1/2}}\right)\left(\frac{\exp[-\kappa_d(\rho^2 + d^2)^{1/2}]}{(\rho^2 + d^2)^{1/2}}\right) \tag{1}$$

where $\kappa_d^2 = 3\mu_a(\mu_s' + \mu_a)$. P_0, μ_s', μ_a, d, and ρ stand for the area-adjusted optical power of a point source, the reduced scattering coefficient, the absorption coefficient, the depth of a point source, and the radial distance in the cylindrical coordinate system, respectively.

Algorithm 1 is introduced to generate a PSF matrix associated with a specific depth and model coefficient. This algorithm addresses the challenges of scattering effects, which often lead to image blur during transillumination. By incorporating key parameters such as the reduced scattering coefficient (μ_s'), absorption coefficient (μ_a), depth (d), and image dimensions, the proposed algorithm aims to generate a PSF matrix tailored to specific imaging conditions.

Algorithm 1 PSF calculation algorithm.

Input: Scattering coefficient (μ_s'), absorption coefficient (μ_a), depth (d), image dimensions (X, Y), and pixel length (L);
Output: PSF matrix (P);
Initialization:
  Calculate the absorption parameter (κ_d): $\kappa_d = [3 \cdot \mu_a \cdot (\mu_s' + \mu_a)]^{1/2}$;
  The incident light intensity (P_0) is set to 1;
  Determine the origin coordinates (X_0 and Y_0) of the image;
  Initialize a matrix P to store the PSF;
PSF calculation, for each pixel (x, y) in the image:
  for $y = 1$ to Y :
    for $x = 1$ to X :
      $\mathrm{rho} = \{[(x - X_0) \cdot L]^2 + [(y - Y_0) \cdot L]^2\}^{1/2}$ # Calculate the radial distance (rho) from the origin;
      $\mathrm{rhod} = (\mathrm{rho}^2 + d^2)^{1/2}$ # Calculate radial distance with depth (rhod);
      $p_1 = \kappa_d + \frac{1}{\mathrm{rhod}}$ # Compute intermediate parameters;
      for PSF (p_1, p_2, p_3):
        $p_2 = d \cdot \frac{1}{\mathrm{rhod}}$
        $p_3 = \frac{e^{-\kappa_d \cdot \mathrm{rhod}}}{\mathrm{rhod}}$
        $P(y,x) = \frac{3 \cdot P_0}{(4\pi)^2}\left((\mu_s' + \mu_a) + (p_1 \cdot p_2)\right) \cdot p_3$ # Update the PSF matrix P using the calculated values;
Normalization: Normalize the PSF matrix P to ensure the sum of its elements equals 1;
File handling:
  Generate a filename for the PSF based on the parameters (μ_s', μ_a, d);
  Save the PSF in the CSV and TIFF formats.

The initialization phase involves computing the absorption parameter (κ_d), setting the incident light intensity (P_0), and establishing the origin coordinates for the image. The subsequent calculation of the PSF for each pixel employs mathematical expressions to account for the radial distances, absorption effects, and the overall intensity distribution. The normalization step ensures that the resulting PSF matrix is scaled appropriately for practical applications.

The validity of the diffusion approximation is based on the requirement that the thickness of the scattering medium significantly exceeds the average free path length of $1/\mu_s'$. Therefore, caution is warranted when using Equation (1) when $(\rho^2 + d^2)^{1/2}$ does not exceed $1/\mu_s'$[14]. Consequently, generating an image with sufficient width for training proves to be more effective in ensuring a result with a profoundly absorbing structure. The light distribution on the surface exhibits a Gaussian-like shape. To calculate the distribution of the deepest source of light points in a turbid medium using Equation (1), the extension of the PSF has to be set appropriately. Figure 3 shows the similarity and the difference of the PSF compared with Gaussian functions. It also shows that the extension of the PSF should exceed about three times the standard deviation for appropriate convolution operations.

Figure 4 shows the PSF-margin setting steps to ensure the proper performance of Algorithm 1 at the image boundaries, the PSF is initially assumed to be obtained on an infinite plane. This is simulated by embedding the PSF in a zero matrix significantly larger than the size of the PSF (more than 3σ), as shown in Fig. 4(a). The intensity values of the PSF are then mapped onto this zero matrix, resulting in the distribution shown in Fig. 4(b). The image is cropped to the target dimensions ($\pm 3\sigma$), as shown in Fig. 4(c). When calculating the deepest light point source distribution in a turbid medium using Equation (1), the image dimensions in each axis should be at least three times the standard deviation of the light intensity distribution across the medium's surface.

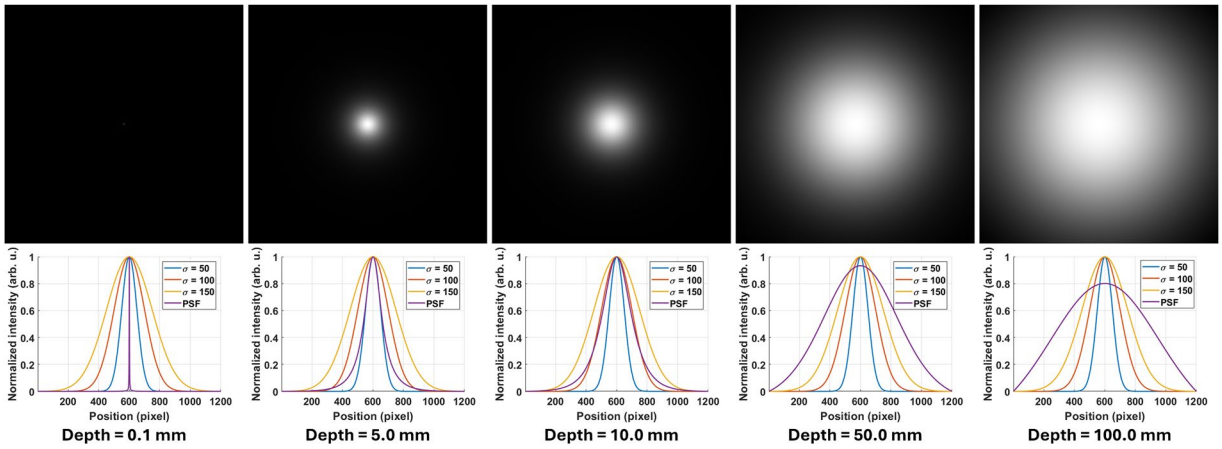

Fig. 3 Images of PSF and their intensity profiles (purple) across the horizontal center line for scattering media with different depth compared with Gaussian profiles with different standard deviations; σ(blue), 2σ (orange), and 3σ (yellow).

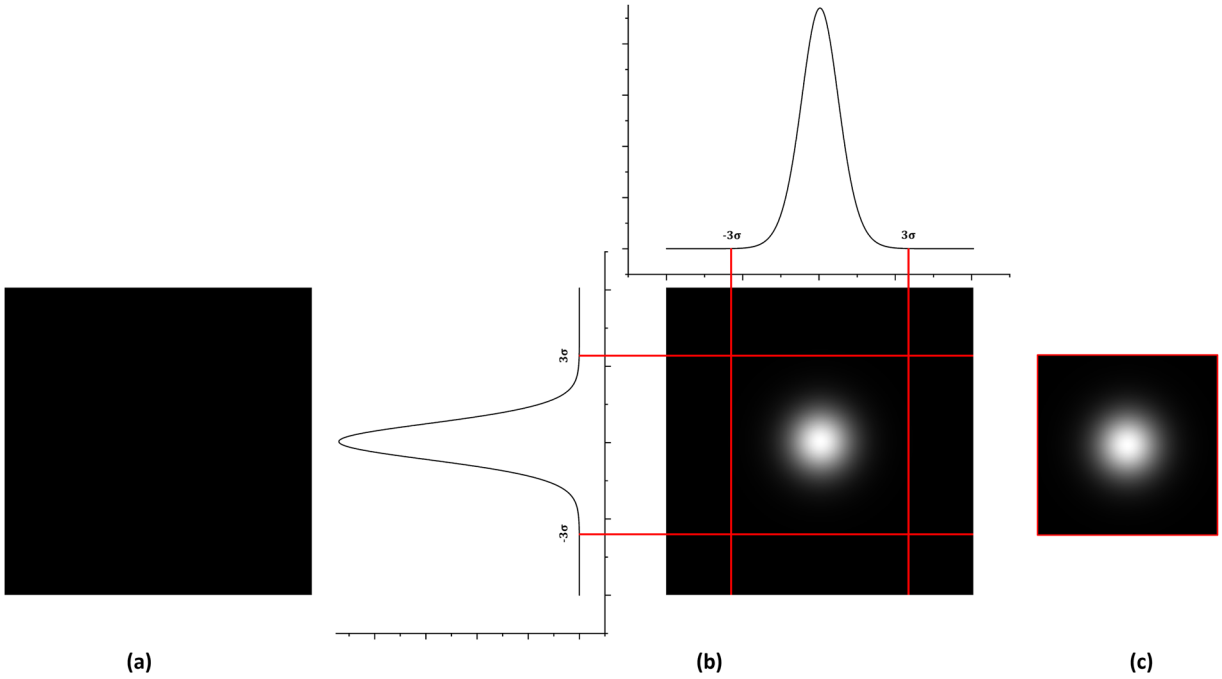

Fig. 4 PSF reconstruction steps to ensure boundary performance: (**a**) image acquisition plane assumed infinite, (**b**) PSF intensity mapping onto the plane, (**c**) lipped PSF with appropriate margin.

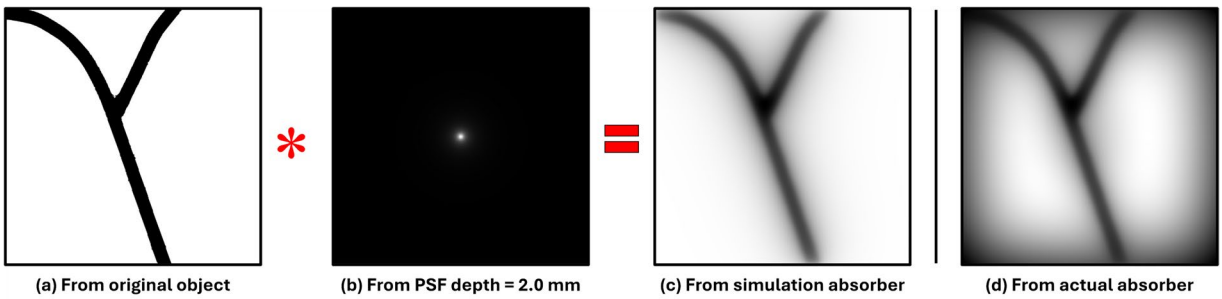

Fig. 5 Simulation of the transillumination image: (**a**) original image of a light-absorbing structure, (**b**) PSF, (**c**) result of 2-dimensional convolution, (**d**) actual image in measurement.

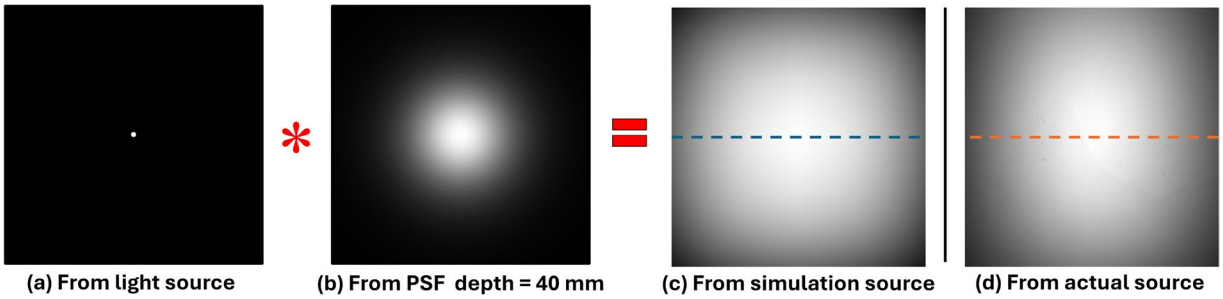

Fig. 6 Simulation of a background in a transillumination image: (**a**) light source distribution at the incident surface of a scattering medium, (**b**) PSF at a maximum depth (thickness of the medium), (**c**) result of PSF convolution, (**d**) measured image at the output surface of a scattering medium[13]. The intensity profiles along broken lines agree well as shown in Fig. 15.

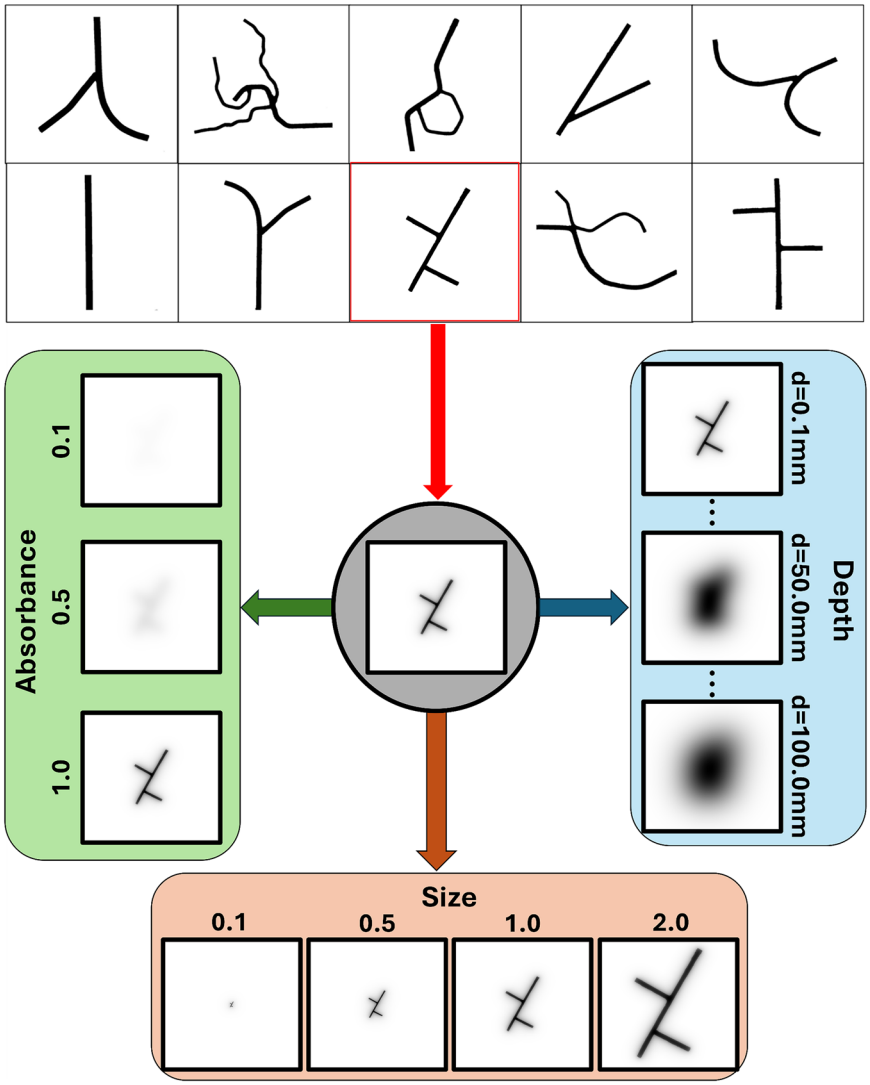

Fig. 7 Overview of the dataset with 10 shapes, each with 4 sizes, 3 absorbances, and 100 depths.

Elimination of Background Effect in Transillumination Images. Figure 5 shows the simulation of a transillumination image using the convolution method. If the background of an original image is uniform (Fig. 5(a)), the convolution with a PSF (Fig. 5(b)) results in an ideal image (Fig. 5(c)). However, in practice, the light source is spatially finite and its illumination is generally non-uniform. It makes the background of the

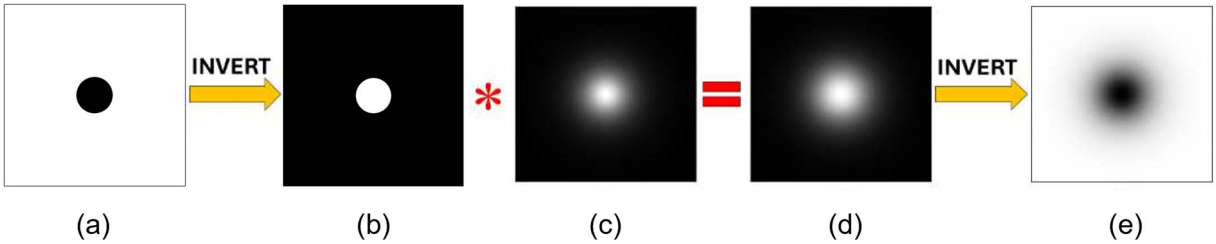

Fig. 8 Simulation of blurred images in transillumination imaging: (**a**) original blur-less image of an absorber, (**b**) B&W inversion, (**c**) PSF distribution, (**d**) blurred fluorescent image, and (**e**) absorber image blurred in transillumination imaging.

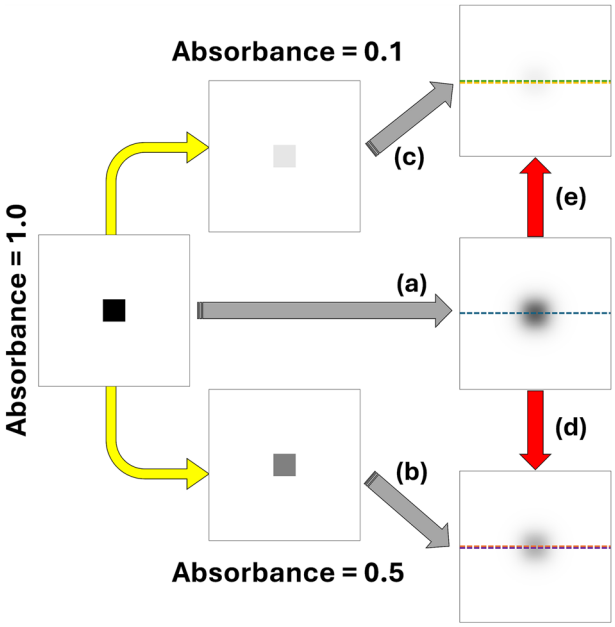

Fig. 9 Two methods to generate transillumination images with different absorbances: In the method 1, blur-less images with an absorber of different absorbance are generated first (yellow arrows). Then, PSF convolution is applied to each blur-less image (gray arrows, processes (**a**), (**b**) and(**c**)); In the method 2, The result of the convolution with a unit absorbance (**a**) is multiplied by the corresponding absorbances (red arrows, processes (**d**) and (**e**)). The computational effort in method 2 is less than method 1.

image inhomogeneous (Fig. 5(d)). This effect can be eliminated by dividing the transillumination image by the background light distribution[13].

Figure 6(a) shows the simulation of the light source distribution was performed by convolutional integration of the light source image, including size and shape, with the PSF as shown in Fig. 6(b) with the maximum depth of the survey medium, as shown in Fig. 6(c). In practice, acquiring the distribution of light sources is difficult as shown in Fig. 6(d).

Equation (2) shows the process of the background calculation by setting the depth of the PSF as the maximum depth or the thickness of the scattering medium μ_s'.

$$I_b(x, y) = I_s(x, y) * PSF(x, y; d = d_{max}) \quad (2)$$

where I_b, I_s, d, d_{max}, * refer to the background light distribution, light source distribution at the illuminated surface of the turbid medium, depth of the absorber in the turbid medium, thickness of the turbid medium, and convolution operation, respectively. Figure 6 shows the simulation of the background distribution using Equation (2)[13].

Absorbers. In previous studies by our group, data diversity was applied to represent the generality of different absorption structures, including their shape, depth, size, and absorption level of the absorbers. In terms of shape, the shapes simulated the structure of blood vessels, including 10 different shapes. In practical measurements, images were acquired with a CCD camera (ORCA-R2 C10600; Hamamatsu Photonics K.K.). The composition of the image dataset is shown in Fig. 7.

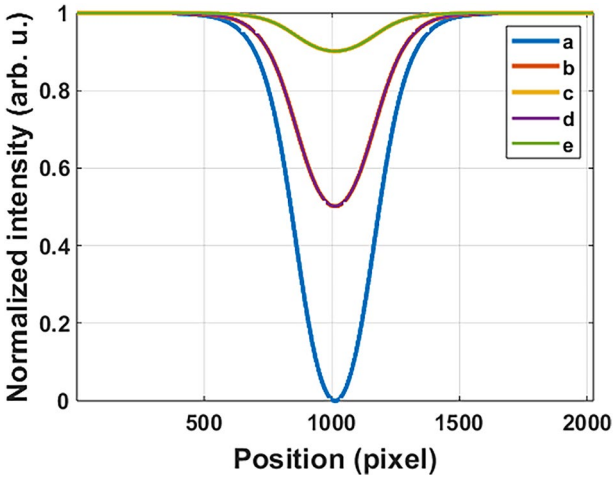

Fig. 10 Absorption intensity profiles from two transillumination imaging methods at different absorbances.

Image processing for blur in transillumination imaging Fig. 8 shows the method to simulate both absorption and fluorescence images using the same dataset shown in Fig. 7. An absorption image (Fig. 8(a)) is converted into a fluorescent image (Fig. 8(b)). By the two-dimensional convolution with PSF (Fig. 8(c)), the blurred image (Fig. 8(d)) through a scattering medium is calculated. An absorption image blurred in transillumination imaging (Fig. 8(e)) is obtained by by converting the blurred fluorescent image (Fig. 8(d)). The bidirectional nature of this process and the validity of this method have been demonstrated by Tran *et al.*[11].

Algorithm 2 Fluorescence and absorption image simulation method.

Input: Two-dimensional matrix of blur-less absorption image, PSF matrix, size of image;
Output: Fluorescent or absorption image blurred in transillumination imaging;
Initialization:
Load blur-less absorption image data and corresponding PSF;
If the image is in color, it is monochromatized;
Adjust the image for image processing;
Preprocessing:
Normalize the pixel values of the loaded image to the range [0, 1];
Adjust the image size by clipping or padding for the convolution with PSF. The extension of PSF matrix should be larger than 3σ, where σ is the standard deviation of PSF distribution;
Convolution:
Convert the absorption image by black-and-white inversion, or subtract the image matrix from an identity matrix with all elements equal to 1;
Convolve the normalized blur-less image with the normalized PSF, obtaining a blurred image;
Size restoration:
Restore the image size to the original by clipping or padding;
Conversion:
If a fluorescent image is required;
Save the matrix as a blurred fluorescent image;
Else:
Convert the image by the black-and-white inversion processing;
Save the matrix as an absorption image;
End.

As mentioned above, two-dimensional convolutions with the widely distributed PSFs require sufficient margins around the 2D matrices to ensure accurate computation. In other words, an infinite viewing area would be ideal for accommodating all depths in a scattering medium; however, this is impractical in practice. In our algorithm, the matrix size is adjusted to three times the standard deviation of the PSF distribution by either clipping or padding the matrix margins. After the convolution operation, the image is restored to its original size through clipping or padding.

To incorporate absorber images with different absorbances into the database, absorption images are processed as shown in Fig. 9. The process starts from the original image, that is 2025 × 2025 pixels image with a 300 pixels per side square at the center. The absorbance values of the peripheral and central parts are 0 and 1, respectively.

Here, for simplicity, we present only two representative absorbances, 0.1 and 0.5. The absorber images with different absorbance are obtained by simply multiplying the element-by-element values of the original matrix by the corresponding absorbances. This process is represented by Equation (3) and the yellow arrows in Fig. 9.

$$A_i(x, y) = A_0(x, y) * i \tag{3}$$

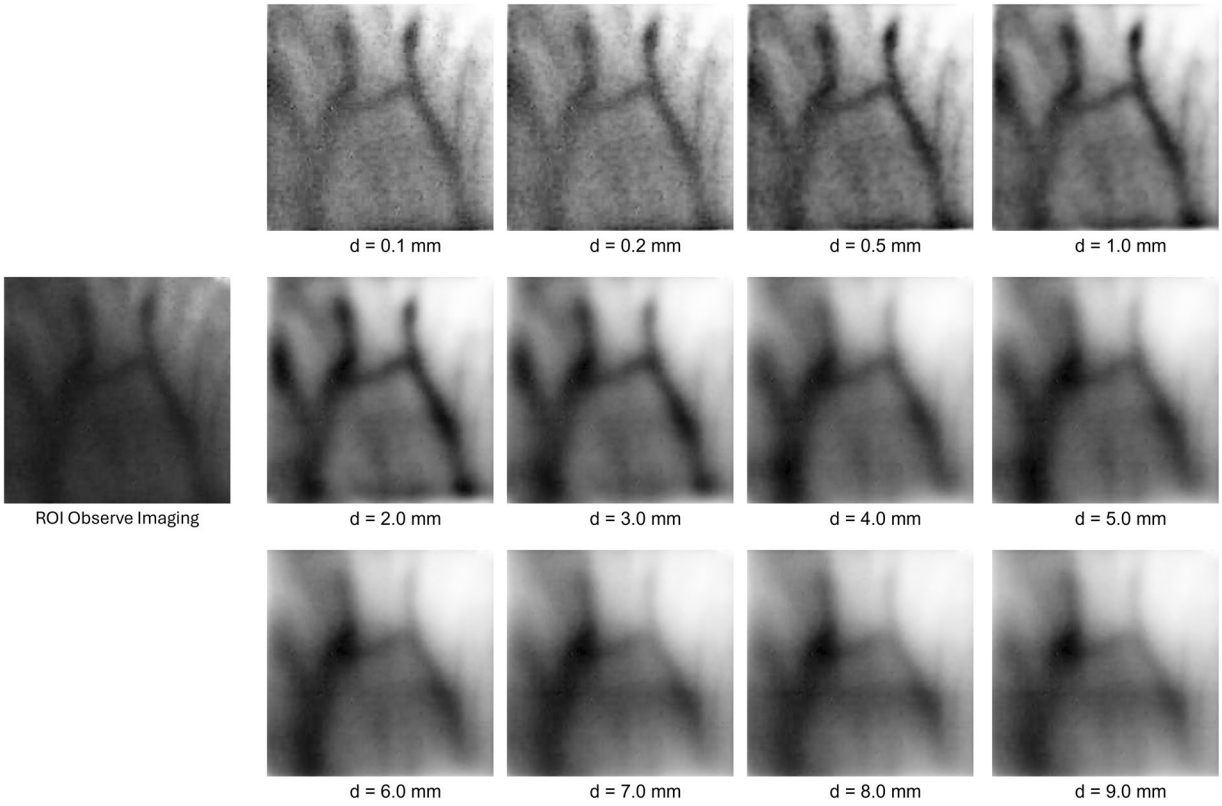

Fig. 11 Example of application of scattering deblurring in biological tissue (blood vessels) when deconvolution with PSF at depths from 0.1 mm to 9.0 mm.

Parameters	Value
Number absorber of shapes	10 shapes
Scattering coefficient of medium	1.0 [mm^{-1}]
Absorption coefficient of medium	0.00536 [mm^{-1}]
Depth range	0.1 - 10.0 [mm]
Relative absorber sizes	0.1, 0.5, 1.0, and 2.0
Relative absorbance of absorber	0.1, 0.5, and 1.0
Image size	2025 × 2025 pixels

Table 1. Parameters and values for the dataset.

where A_i, A_0, and i are the structure matrix with absorbance i, matrix with absorbance structure 1.0, and absorbance, respectively.

Next, we simulate the blurred images by the convolution with the PSF. Figure 9 shows an example of the convolution process for different absorbances. The conditions of this example are: object depth 15.0 mm, $\mu_a = 0.00536$ mm^{-1}, $\mu_s' = 1.0\,mm^{-1}$, 10 pixels/mm resolution. The convolution process is presented in Algorithm 2. This process corresponds to the gray arrows ((a), (b) and (c)) in Fig. 9. The blurred images well represent the difference of the absorber absorbances.

Since the convolution is a linear operation, this process can be simplified as follows. First, we obtain the blurred image from the original image with the intensity 1 absorber (process (a)). Then, we can obtain the blurred images by simply multiplying the resultant image by corresponding absorbances using the same Equation (3) (processes (d) and (e)). In this way, we can make computational effort less, which is often meaningful in large data-base computation. Digital computation of convolution includes the approximation for integral operations. The effect of such errors in the proposed two methods was checked.

Figure 10 shows the result of a numerical check for these two methods. The good agreement among intensity profiles along the central horizontal line (broken lines in Fig. 9) was confirmed with sufficiently low deviations. In deep learning, particularly in supervised learning of image-to-image correspondence, the absorbance-weighted original images are required. The first method mentioned above can provide both blur-less and blurred images for the training pairs in deep learning. On the other hand, in other applications such as image classification and image semantic determination, the original images are not necessary. For example, we can estimate the absorber depth in a scattering medium from a blurred image by learning the correspondence between the depth and the

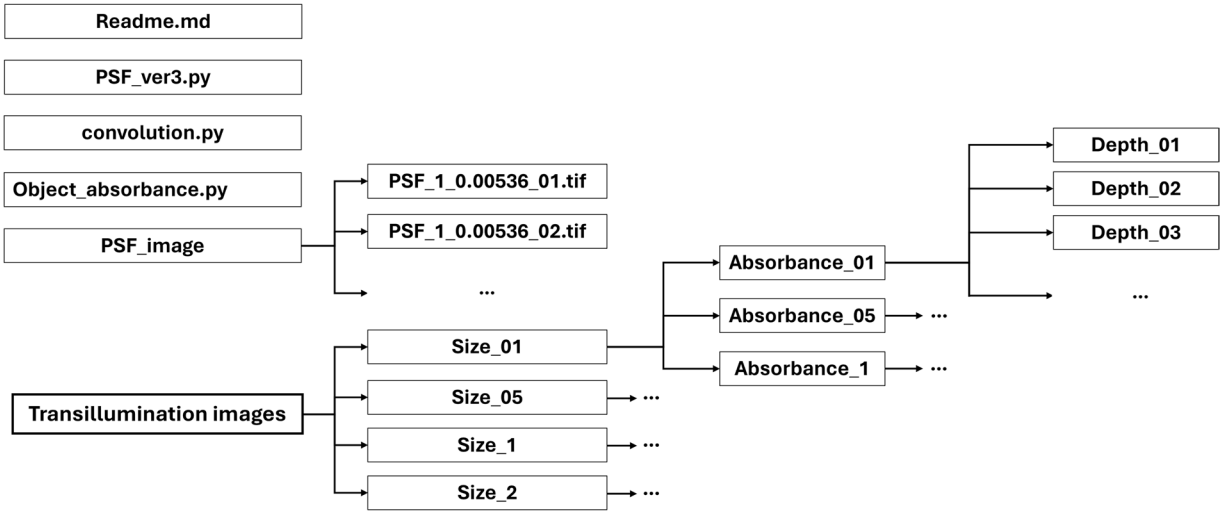

Fig. 12 Directory structure of dataset.

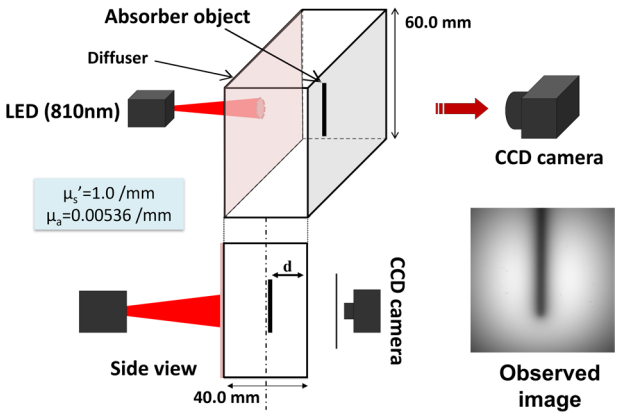

Fig. 13 Experimental setup for the validation of background effect elimination. d_{max}.

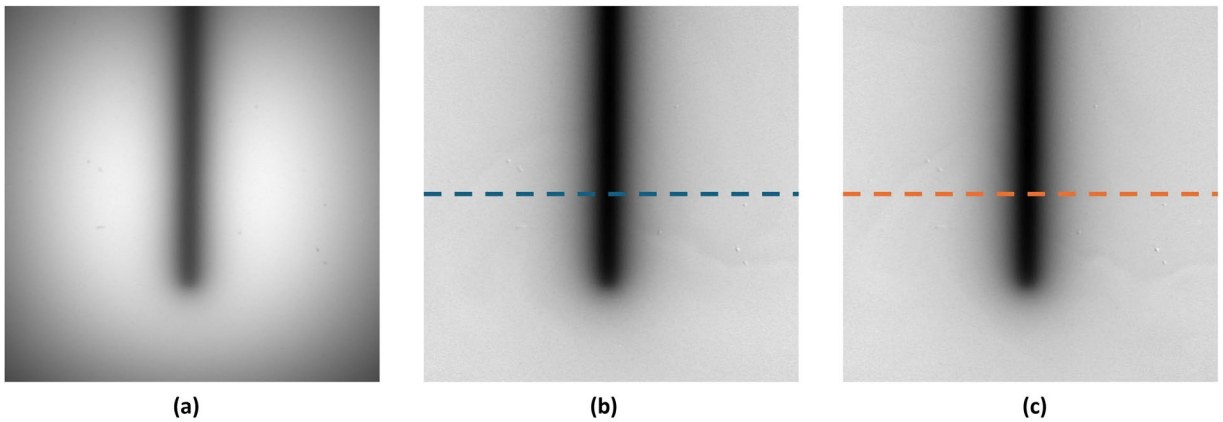

Fig. 14 Background removal technique by dividing the observed transillumination imaging (**a**) with the actual background (**b**) and the background from the PSF (**c**).

image-blur[13]. In such an application, the second method can provide large amount of training pairs efficiently. If the absorber depth in the blurred transillumination image can be estimated, a blur-free image can be obtained through deconvolution using the PSF corresponding to the estimated depth. Figure 11 illustrates the variation in deconvolution results when using PSFs of different depths, highlighting the dependence of subcutaneous

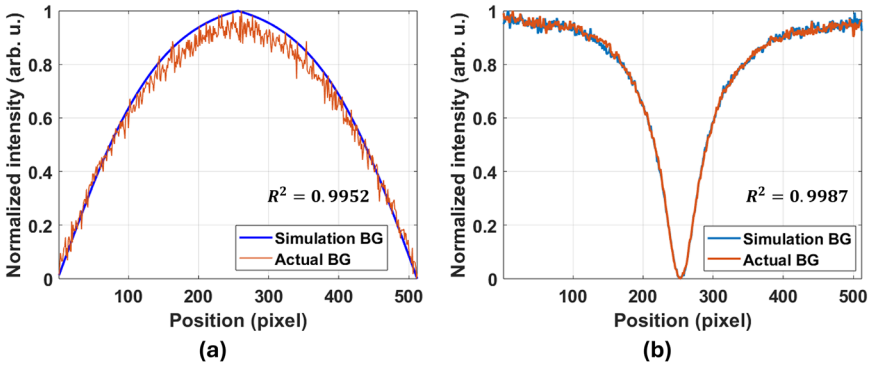

Fig. 15 Comparison of intensity profiles for background removal: (**a**) simulated background using PSF (Fig. 6(c)) and actual background (Fig. 6(d)); (**b**) result images after removal of simulated and actual backgrounds (Fig. 14(b) and (c)).

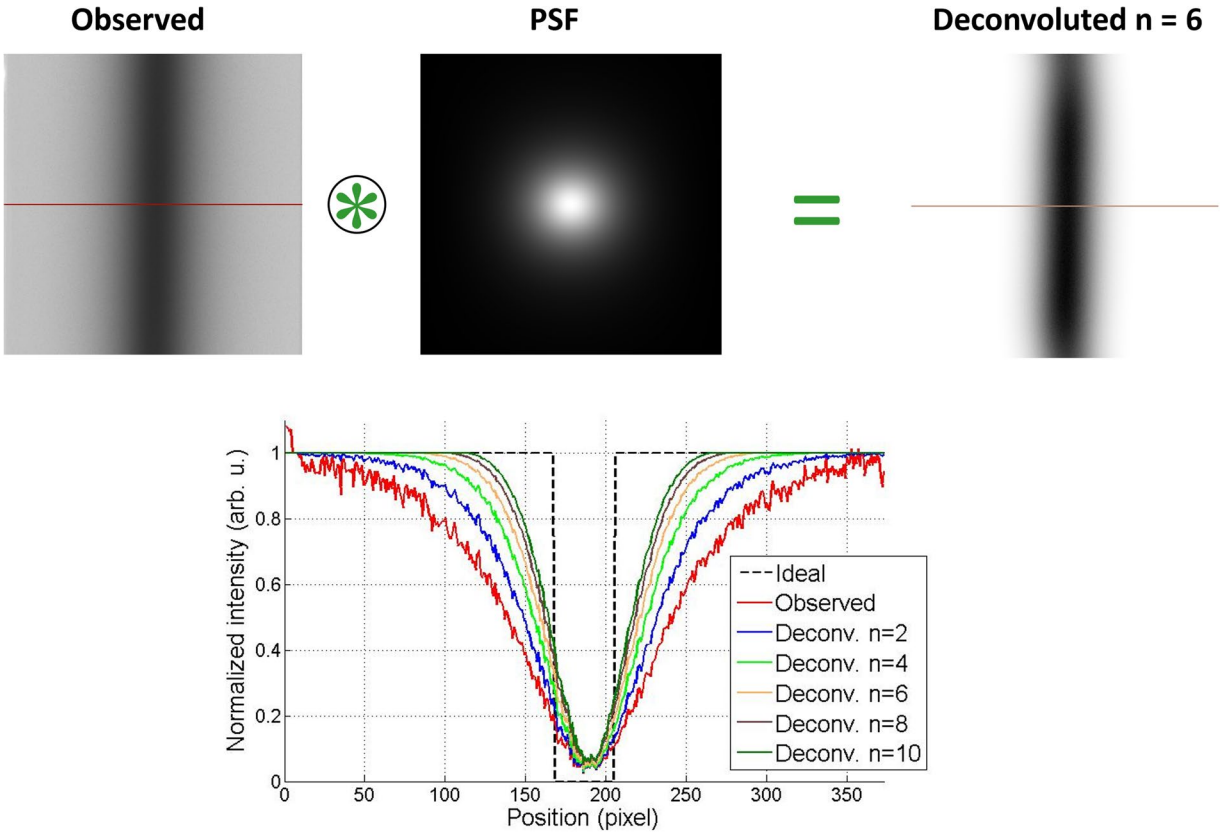

Fig. 16 Image deblurring by PSF deconvolution: ⊛and n refers to deconvolution operation and the number of deconvolution iteration, respectively.

vein clarity on the deconvolution depth. By applying this principle, a blur-free three-dimensional image can be reconstructed from a single blurred transillumination image[13]. This experiment was conducted with an array of 940 nm wavelength IR-LEDs, AE-LED56V2, Akizuki-denshi and CCD camera (Ruishikeni).

Data Records

This study used a sample dataset with optical and imaging parameters, as detailed in Table 1. It includes ten different absorber shapes, as shown in Fig. 7. The reduced scattering and absorption coefficients of the scattering medium were respectively set to 1.00 mm^{-1}, and 0.00536 mm^{-1} to simulate the environment for near-infrared light in Intralipos solution. The absorber depth ranges from 0.10 mm to 10. mm, with increments of 0.10 mm, resulting in a total of 100 different depths. There are four kinds of relative absorber sizes: 0.10, 0.50, 1.0, and 2.0,

and three kinds of relative absorbances: 0.10, 0.50, and 1.0. The resolution value was set to. The image size and resolution were set to 2025 × 2025 pixels and 10 pixels/mm, respectively. Consequently, the total number of sample images was 12,000.

Figure 12 shows the following three algorithm files and folders in directory trees.

- `The file PSF_ver3.py` contains the algorithm for generating the PSF matrix based on Equation (1);
- `The file convolution.py` contains the algorithm for convolving an original image with a PSF to simulate a transillumination image of an absorber or fluorescence in a scattering medium;
- `The file Object_absorbance.py` contains the algorithms for generating images of various absorbers structures in air and scattering media;

The folders contain PSF images and transillumination images with various absorber sizes, `Size_01`, `Size_05`, `Size_1`, and `Size_2`, each with various relative absorbances (`Absorbance_01`, `Absorbance_05`, and `Absorbance_1`), each with various depths from 0.1 mm to 10.0 mm (`Depth_01`, `Depth_02`,..., `Depth_10.0`). The image files were named according to the rule "Object_order_object_size_absorbance_depth.png.". Consequently, we offer a dataset of transillumination images with 100 depths ranging from 0.1 mm to 10.0 mm, step 0.1 mm; four sizes of 0.1, 0.5, 1.0, and 2.0; and three absorbances of 0.1, 0.5, and 1.0[18].

Technical Validation

The effectiveness of eliminating the background effect of the light source was validated through the experiment shown in Figure 13. The scattering medium was an Intralipid suspension ($\mu_s' = 1.0\ \mathrm{mm}^{-1}$, $\mu_a = 0.00536\ \mathrm{mm}^{-1}$, Otsuka Pharmaceutical Co. Ltd.). An absorber was placed at a depth of $d = 10$ mm, and the inner wall distance of an acrylic tank was $d_{\max} = 40$ mm. An LED light source with 810 nm wavelength (OSLUX IR, PowerStar; EMSc UK Ltd.) was expanded through a diffuser for homogeneous illumination. An image is obtained using a cooled CCD camera (ORCA-R2 C10600; Hamamatsu Photonics K.K.) oriented toward the opposite face of the phantom to the light-incident side.

Figure 14 shows the results of the experiment to examine the validity of the background effect removal. Figure 14(a),(b) and (c) respectively show the measured transillumination image, removal with an actual background (corresponds to Fig. 6(d)), and removal with the simulated background (corresponds to Fig. 6(c)).

Figure 15(a) shows the comparison between the actual and simulated backgrounds in the normalized intensity profiles along the central horizontal position of the simulated (Fig. 6(c)) and actual background (Fig. 6(d)). Figure 15(b) shows the normalized intensity profiles along the central horizontal positions of the image after the background removal (Fig. 14(b),(c)). The results show a good agreement between the cases with the actual and simulated backgrounds. This suggests the validity of the proposed technique, or the background effect can be removed using the PSF with the thickness of a scattering medium.

Usage Notes

When applying the proposed technique to fluorescence images, the user should skip the first inversion process in the "Convolution" section in the Algorithm 2. The transilluminated fluorescent images can be obtained before the final inversion process in the Algorithm 2.

The imaging-planee size should be more than three times the standard deviation of PSF at the maximum depth of a scattering medium when calculating the by Equation (1).

The PSF-deconvolution process for images deblurring can introduce a positional deviation of one pixel between the original and resulting images. This deviation arises from the fast Fourier transform used in the algorithm and the Richardson-Lucy deconvolution iterations. Although it is imperceptible in an overall visual observation, caution is required when performing image calculations such as division. Figure 16 illustrates the positional offset, an example of a deblurred image, and the effects of iteration in the deconvolution process[11,19].

Code availability

We provide a codebase designed to produce the PSFs, construct fluorescence or absorption images with varying physical and optical parameters. https://github.com/HoangNhutHuynh/A-large-open-access-dataset-of-transillumination-image.git.

Received: 28 June 2024; Accepted: 12 February 2025;
Published: 6 March 2025

References

1. Rao, J., Dragulescu-Andrasi, A. & Yao, H. Fluorescence imaging in vivo: recent advances. *Curr. Opin. Biotechnol.* **18**, 17–25, https://doi.org/10.1016/j.copbio.2007.01.003 (2007).
2. Shimizu, K. Near-infrared transillumination for macroscopic functional imaging of animal bodies. *Biology* **12**, 1362, https://doi.org/10.3390/biology12111362 (2023).
3. Yang, K. *et al*. Data-driven polarimetric imaging: a review. *Opto-Electron. Sci.* **3**, 230042–1, https://doi.org/10.29026/oes.2024.230042 (2024).
4. Key, H., Jackson, P. C. & Wells, P. N. T. New approaches to transillumination imaging. *J. Biomed. Eng.* **10**, 113–118, https://doi.org/10.1016/0141-5425(88)90084-2 (1988).
5. Taka, Y., Kato, Y. & Shimizu, K., Transillumination imaging of physiological functions by NIR light. In *Proc. 22nd Annu. Int. Conf. IEEE Eng. Med. Biol. Soc.***1**, 771-774, https://doi.org/10.1109/IEMBS.2000.900863 (2000).
6. Amaechi, B. T., Owosho, A. A. & Fried, D. Fluorescence and near-infrared light transillumination. *Dent. Clin. North Am.* **62**, 435–452, https://doi.org/10.1016/j.cden.2018.03.010 (2018).

7. Liang, S. & Shimizu, K. Development of a technique to measure local scattering in turbid media using backscattered light at the surface for noninvasive turbidity evaluation of blood in subcutaneous blood vessels. *Jpn. J. Appl. Phys.* **60**, 022002, https://doi.org/10.35848/1347-4065/abd36a (2021).
8. Cuper, N. J. *et al.* The use of near-infrared light for safe and effective visualization of subsurface blood vessels to facilitate blood withdrawal in children. *Med. Eng. Phys.* **35**, 433–440, https://doi.org/10.1016/j.medengphy.2012.06.007 (2013).
9. Papaioannou, D. G., Baselmans, J. J. M. & Van Gemert, M. J. C. Image quality in time-resolved transillumination of highly scattering media. *Appl. Opt.* **34**, 6144–6157, https://doi.org/10.1364/AO.34.006144 (1995).
10. Shimizu, K., Tochio, K. & Kato, Y. Improvement of transcutaneous fluorescent images with a depth-dependent point-spread function. *Appl. Opt.* **44**, 2154–2161, https://doi.org/10.1364/AO.44.002154 (2005).
11. Tran, T. N., Yamamoto, K., Namita, T., Kato, Y. & Shimizu, K. Three-dimensional transillumination image reconstruction for small animals with a new scattering suppression technique. *Biomed. Opt. Express* **5**, 1321–1335, https://doi.org/10.1364/BOE.5.001321 (2014).
12. Schwendicke, F., Elhennawy, K., Paris, S., Friebertshäuser, P. & Krois, J. Deep learning for caries lesion detection in near-infrared light transillumination images: a pilot study. *J. Dent.* **92**, 103260, https://doi.org/10.1016/j.jdent.2019.103260 (2020).
13. Van, T. N. P., Tran, T. N., Inujima, H. & Shimizu, K. Three-dimensional imaging through turbid media using deep learning: NIR transillumination imaging of animal bodies. *Biomed. Opt. Express* **12**, 2873–2887, https://doi.org/10.1364/BOE.420337 (2021).
14. Dang, N. N. A., Huynh, H. N. & Tran, T. N. Improvement of the performance of scattering suppression and absorbing structure depth estimation on transillumination image by deep learning. *Appl. Sci.* **13**, 10047, https://doi.org/10.3390/app131810047 (2023).
15. Dang, N. N. A., Huynh, H. N., Tran, T. N. & Shimizu, K. Reconstructing 3D de-blurred structures from limited angles of view through turbid media using deep learning. *Appl. Sci.* **14**, 1689, https://doi.org/10.3390/app14051689 (2024).
16. Huynh, H. N., Bui, P. A., Dam, P. A., Tran, A. T. & Tran, T. N. Scattering suppression of transillumination images using deep learning for 3D reconstruction of light absorbing structures in turbid medium. In. *Comput. Opt. Imaging Artif. Intell. Biomed. Sci.* **12857**, 116–124, https://doi.org/10.1117/12.3004898 (2024).
17. Wang, J., Shimizu, K. & Yoshie, O. Transformer connections: improving segmentation in blurred near-infrared blood vessel image at different depths. *IEEJ Trans. Electr. Electron. Eng.* **19**, 1828–1841, https://doi.org/10.1002/tee.24146 (2024).
18. Van, T. N. P., Huynh, H. N., Dang, N. N. A., Tran, T. N. & Shimizu, K., A large open access dataset of transillumination imaging toward realization the optical computed tomography. *Figshare* https://doi.org/10.6084/m9.figshare.27457908 (2024)
19. Perez, V., Chang, B.-J. & Stelzer, E. H. K. Optimal 2D-SIM reconstruction by two filtering steps with Richardson-Lucy deconvolution. *Sci. Rep.* **6**, 37149, https://doi.org/10.1038/srep37149 (2016).

Acknowledgements

The authors are grateful to Prof. Yuji Kato, Hokkaido University, Japan, and Prof. Takeshi Namita, Shibaura Institute of Technology, for their contributions and advice at the beginning of this study. We acknowledge Ho Chi Minh City University of Technology (HCMUT), VNU-HCM for supporting this study.

Author contributions

K.Shimizu and T.N.Tran proposed the conceptualization and methodology; V.T.N.Phan and T.N.Tran conceived and conducted the experiments; V.T.N.Phan, N.N.A.Dang, and H.N.Huynh conducted the data curation, analysis, investigation, and validation; T.N.Tran and K.Shimizu provided resources; V.T.N.Phan and H.N.Huynh wrote the original draft preparation and made the visualization; K.Shimizu and T.N.Tran reviewed and edited. All authors have read and agreed to the published version of the manuscript.

Competing interests

The authors declare no competing interests.

Additional information

Correspondence and requests for materials should be addressed to T.N.T. or K.S.